Cellulose
https://doi.org/10.1007/s10570-024-06136-9

ORIGINAL RESEARCH

Molecular-engineered cotton textile with multimodal heating and high robustness for personal thermal management

Benhui Li · Shuyu Ao · Haibo Song · Chong Liu · Fengxin Sun · Xuzhong Su

Received: 15 January 2024 / Accepted: 20 August 2024

Abstract Developing natural cotton textiles in personal thermal management applications is of great significance for defending human against adverse climate conditions. However, the intrinsic low optical energy conservation of cotton in terms of human mid-infrared radiation and solar spectrum prevents it from realizing high-efficient thermal retention. Herein, by leveraging a facile technique involving polydopamine (PDA)-assisted ion deposition, we firmly embed silver nanoparticles onto cotton fibers, creating silver-nanoprocessed cotton fabrics (Ag-fabric) with high human mid-infrared reflectivity and superior water/wear resistance. Meanwhile, the localized surface plasmon resonance effect of the PDA and silver nanoparticles contributes to high solar spectrum absorptivity. The as-prepared Ag-fabric demonstrates nearly 2 °C higher temperature compared to unadorned cotton fabrics due to enhanced human mid-infrared radiation, and the outdoor tests show a temperature increase of average 8 °C when covering artificial skin. Moreover, the uniformly distributed silver nanoparticles on hierarchically assembled cotton fibers endow the Ag-fabric with desirable Joule heating performance (~40.7 °C at 1 V), self-cleaning capacity, and antibacterial properties, while maintaining breathability and comfort. These merits of the Ag-fabric present promising advantages to transfer natural cotton into commercially available thermal management wearables and eco-textiles.

Keywords Passive radiative heating · Personal thermal management · Cotton fabrics · Infrared reflection · Durability · Multifunction

Supplementary Information The online version contains supplementary material available at https://doi.org/10.1007/s10570-024-06136-9.

B. Li · S. Ao · F. Sun (✉) · X. Su (✉)
Key Laboratory of Eco-textiles of Ministry of Education, Jiangnan University, Wuxi 214122, China
e-mail: fxsun@jiangnan.edu.cn

X. Su
e-mail: mfgucv@163.com

H. Song · C. Liu
Shenzhen Purcotton Technology Co., Ltd., Shenzhen 518131, China

F. Sun
Laboratory of Soft Fibrous Materials, College of Textiles Science and Engineering, Jiangnan University, Wuxi 214122, China

Introduction

In cold weather, discomfort can occur if the heat produced by the body is not in balance with the surrounding environment, and it can even be life-threatening if the body temperature falls below the human core temperature of 37 °C (Axelrod and Diringer 2006). To maintain thermal comfort, people rely intensively on various heating devices based on electric heat and fossil fuels, which accounts for ~40% of

Published online: 23 August 2024

a household's daily energy consumption (Alves et al. 2016). It is necessary to develop an efficient and environmentally friendly solution to maintain human thermal comfort. Textiles and clothing, as a second skin, have been used to keep human body warm and protect the body from the cold, which focuses on the temperature changes of the human body and its local microenvironment rather than the whole room space. However, conventional garments keep warm by increasing the thickness or layer count to preserve still air within the dress and minimize heat convection (Yue et al. 2019), which contributes unpleasant appearance and reduce wearing comfort. Moreover, the relatively high mid-infrared emissivity and low solar absorption of conventional textiles further reduce their thermal comfort in cold weather.

Recently, researchers have proposed the concept of radiative heating effects for personal thermal management for sustainable energy-saving development (Hong et al. 2019; Hsu et al. 2017; Yang et al. 2023; Zhao et al. 2018). The human body generally dissipates heat to the surrounding environment through thermal radiation, thermal conduction, and air convection. The proportion of these three ways varies depending on the ambient environment. For indoor cases, approximately 50% of the heat emitted by a sedentary body is through thermal radiation at mid-infrared (IR) wavelengths (Peng and Cui 2020). In outdoor situation, although the air convection may increase, the solar radiation provides a superior heat source. Therefore, thermal management textiles with high human mid-infrared reflectivity and solar energy absorption for photothermal conversion have shown great potentials to achieve efficient human body heating. More recently, various radiative heating materials and structures, such as Mxene (Lan et al. 2023), metallic nanowire (Hsu et al. 2015; Tang et al. 2023), and multilayered fibrous membranes (Tian et al. 2021; Wang et al. 2019b), have been reported. However, current advances generally suffer from complicated fabrication and relatively singular heating function (either mid-infrared reflection or solar absorption). Moreover, the building blocks of these textiles are not the comment materials for daily clothing and thus source-limited and expensive, which hinders the scalable production and practical application of these heating textiles in our daily lives.

Cotton has been one of the most commonly used textile materials for centuries, with its excellent skin touch comfort, moisture absorption, and soft and warm sensation (Yang et al. 2003). Similar to polar bear hair (Wu et al. 2023b), cotton shows a natural hollow core in the cellulose shell resulting from its multistage biosynthesis, creating a desirable structure that keeps the air with low thermal conductivity within cotton fibers for warmth. Meanwhile, the self-twisting and curled morphology for a typical cotton fiber also contributes to its instinct loftiness and warm feelings (Fang 2018). Therefore, cotton fibers are considered as a promising material for thermal insulation. However, their application in warm clothing is limited by their high mid-infrared emission and low solar spectrum absorption.

To develop cotton textiles for heating textiles, it is imperative to develop facile and cost-effective strategy to process natural cotton fibers into functional radiative materials. Metals have exhibited desirable infrared reflectivity in various everyday applications (Gao et al. 2017; Li et al. 2023; Wang et al. 2021), wherein silver is an excellent choice among different metallic materials because of its high infrared reflectance efficiency, resistance to acids and bases (Khan et al. 2016). However, current advances in producing radiative textiles typically process the textiles physically via vapor deposition, dip-coating, sputtering and spraying (Karim et al. 2020), resulting in non-durable coating structures due to the low adhesivity and weak interactions. In addition, certain strategies apply dense coatings on textiles, which leads to limited breathability, enhanced rigidity and thus threaten the comfortability of textiles (Gong et al. 2022; Wang et al. 2022; Yue et al. 2020). The contradiction between personal thermal management ability and wearing performance requires the development of cotton textiles with high-performance heating and excellent wearing performance by a facile and efficient strategy.

Herein, we demonstrate a functional cotton textile (namely Ag-fabric) with multimode heating, including indoor radiative heating, outdoor solar absorption heating and electric heating functionalities, based on a nanoprocessed technology via PDA-assisted ion deposition (Fig. 1). The PDA provides anchoring positions for the silver nanoparticles (AgNPs), forming chelation at the molecular level between the catechol groups in PDA and silver ions through dative covalent bonds. This facilitates the uniform generation of AgNPs, thereby forming an infrared

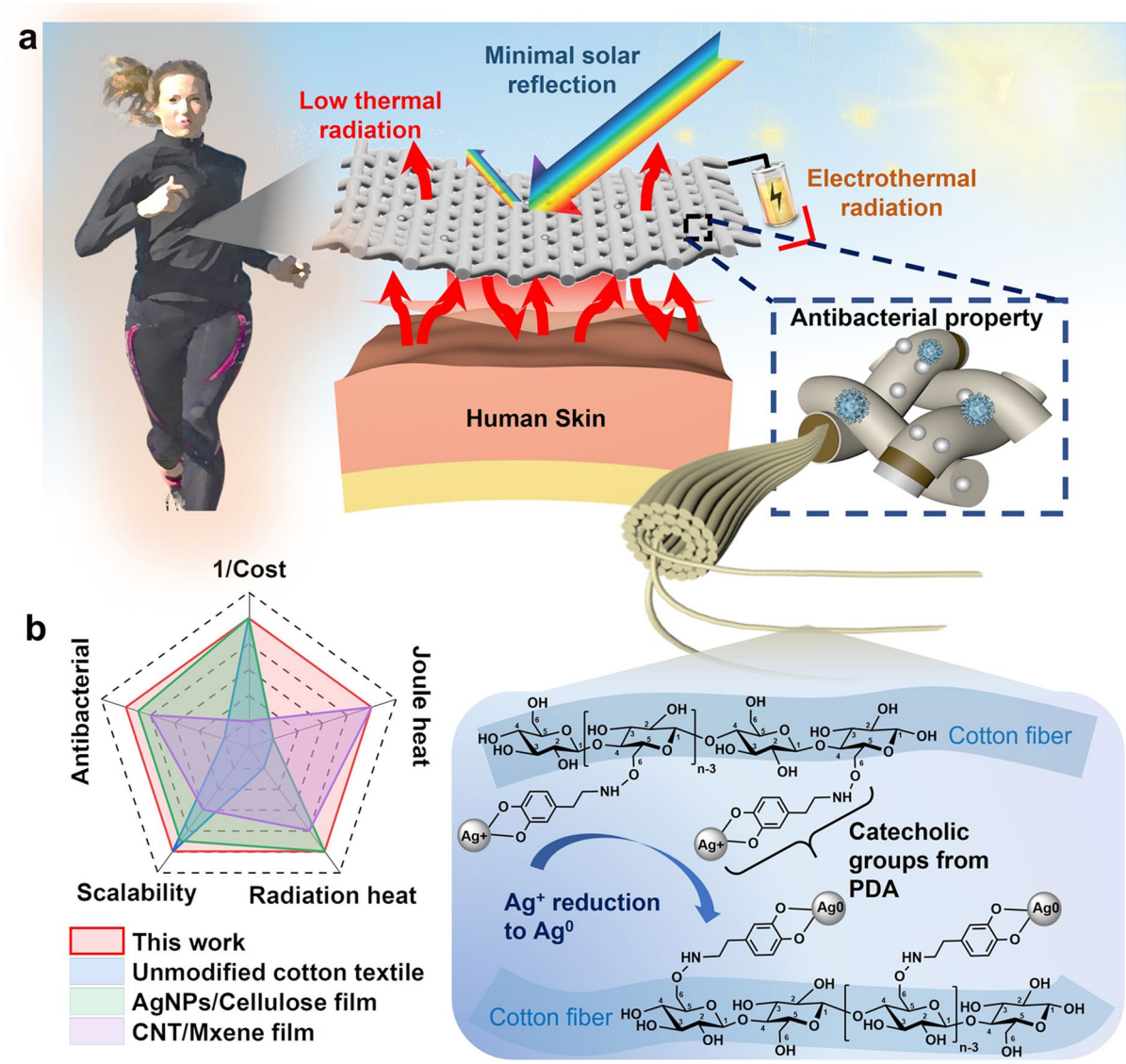

Fig. 1 Schematic illustration of the thermal insulation textile and its performance. **a** Concept note of the thermal insulation cotton fabric via AgNPs chelating with PDA-modified cellulose fibers. **b** Comparisons of the thermal insulation cotton fabric with conventional heating textiles and unmodified cotton textiles

reflective coating which effectively reflects human mid-infrared radiation to achieve a warming effect. In addition, the localized surface plasmon resonance effect of the PDA and AgNPs improved photothermal conversion efficiency of the Ag-fabric. The designed passive heating Ag-fabric exhibits high solar absorption (~80%) and mid-infrared reflectivity (~40%), effectively promoting solar heating and reducing radiant heat dissipation from the human body. Furthermore, the Ag-fabric exhibits excellent Joule heating properties (~40.7 °C at 1 V) due to the conductive nature of the silver nanocoating. The AgNPs are strongly combined with cotton fibers by the synergistic effect of the chelation and PDA adhesion, contributing to the robust heating performance with high durability and wearability, while still maintaining excellent breathability of the Ag-fabrics. Additionally, the fabrication of the Ag-fabric is simple, scalable and cost-effective, and can be applied to different types of cotton fabrics (Fig. 1b and Table S1,

Supporting Information). The advantages of the designed Ag-fabric make it promising for commercial thermal management textile applications.

Experimental section

Materials

Dopamine hydrochloride (DA, 98%), and trimethylolaminomethane (TRIS, 99%) were purchased from Shanghai Titan Technology Company. Silver nitrate ($AgNO_3$), sodium hydroxide (NaOH, 98%), ammonium hydroxide ($NH_3{\cdot}H_2O$, 28%), glucose ($C_6H_{12}O_6$), and hydrochloric acid (HCl, 36%) were purchased from Sinopharm Chemical Reagent Company. All reagents were used as is, without further treatment. The cotton fabrics with thickness of 0.43 mm and weight of 373 g/m^2 were purchased from Shandong Luthai Textile Co., Ltd. (China).

Preparation of PDA-modified cotton fabric

The cotton fabric (3 cm × 3 cm) was washed once with 5 wt% NaOH solution at a temperature of 50 °C for 30 min to remove impurities on the fabric, using a magnetic stirrer at 300 rpm. The cotton fabric was then rinsed several times with deionized water until the wastewater reached neutrality, and then dried in an oven at 40 °C. The buffer solution is prepared by TRIS (0.01 mol), and a 10 mM (millimole) of DA is dissolved in the TRIS buffer. The pH of the solution was adjusted to 8.5 using diluted hydrochloric acid to make the solution slightly alkaline. The cotton fabric was placed in the prepared solution and stirred with a magnetic stirrer at 30 rpm under room temperature for 24 h. Finally, the fabric was washed with deionized water three times and then dried in an oven at 40 °C. The cotton fabrics modified with PDA are referred to as PDA-fabric.

Preparation of silver nanoparticle modified cotton fabric

The $AgNO_3$ particles were dissolved in a certain amount of deionized water and stirred with a glass rod until completely dissolved. Then, aqueous ammonia (NH_3–H_2O) was slowly added dropwise to the $AgNO_3$ solution until it changed from turbid to clear solution. By adjusting the concentration of $AgNO_3$ solution, a series of cotton fabrics with different loadings of AgNPs was prepared, and the silver-attached cotton fabrics were denoted as Ag-fabric-x (x = 4, 6, 10, 12, and 16 g/L), with x representing the mass concentration of $AgNO_3$ solution. The PDA-fabrics were put into silver-ammonia solution and stirred with a magnetic stirrer for 30 min, and then 50 mL of a 5% dextrose solution was added to the silver-ammonia solution and stirred for another 40 min. The treated samples were washed with deionized water several times until the wash water was clear, and then dried in an oven at a temperature of 40 °C.

Material characterizations

Material characterizations

The microscopic morphology was characterized by scanning electron microscopy (SEM, su1510, Hitachi, Ltd., Japan) with an operating voltage of 5 kV. The distribution of AgNPs on the cotton fabric was characterized using energy-dispersive X-ray spectroscopy (EDS) of the SEM system. FT-IR (Nicolet-10, Thermo Fisher Scientific, Inc, USA) was used to analyze the functional groups and chemical bonding of the cotton fabrics and treated samples, and all spectra were calculated from 32 individual scans with a resolution of 1 cm^{-1} and a range of 4000–500 cm^{-1}. The crystal structures were observed using an X-ray diffractometer (XRD, D2 PHASER, Bruker AXS GmbH, Germany) with a diffraction angle range of 5°–90° and a step width of 0.1°, using a Cu Kα diffraction source. The surface elemental composition of the Ag-fabric was determined by X-ray photoelectron spectroscopy (XPS). The binding energies were calibrated to the C 1s peak at 285.0 eV. High-resolution Ag 3d spectra were fitted using Avantage software (Thermo Scientific). The spectral reflectivity ($R(\lambda)$) and transmittance ($T(\lambda)$) in the infrared region (3–20 μm) were determined in a Fourier transform infrared spectrometer (FTIR, Nicolet-10, Thermo Fisher Scientific, Inc., USA) with an integrating sphere. The sunlight reflectivity spectrum (0.3–2.5 μm) was measured by using a UV-VIS-NIR spectrometer with a diffuse integrating sphere (Lambda950, Platinum Elmer, USA). All data measured by the instruments were processed through Origin 2018 or Microsoft Excel 2019 software.

Heating performance test

Radiation heating measurements were performed indoors by placing the rubber on a heating table with a constant temperature of 33 °C as artificial skin, covered by the unadorned cotton fabric (3 cm × 3 cm) and Ag-fabric (3 cm × 3 cm), separately. The temperature evolution was recorded by thermocouples (YET-640X). Three replicates were conducted, and the average of the data was reported. The photothermal conversion test was conducted outdoors on both sunny and cloudy days. The unadorned cotton fabric and Ag-fabric pieces were tested inside a foam box with an open top which was sealed with a transparent polyester film to prevent the effect of air convection during testing. The temperature change under sunlight was recorded by the thermocouples. Considering that a large amount of data versus time can be obtained in a single experiment to demonstrate the temperature differences among different types of fabrics, only one experiment was conducted over a 6-hour duration. For the Joule heating experiment, we used a multimeter (FLUKE F107) to measure the resistance change of Ag-fabric with different silver nitrate concentrations. The resistance data with error bar are represented by mean ± standard deviations based on three replicates. The Ag-fabrics were supplied with current through a DC power regulator, and the temperature rise was recorded by the thermocouples and an infrared thermographer (FLIR-E5-XT).

Wearing performance test

The mechanical properties of the cotton fabric and Ag-fabric with size of 20 mm × 5 mm and thickness of 0.04 mm were investigated experimentally using a universal testing machine (UTM2203). Uniaxial tensile tests were conducted under a gauge length of 100 mm at a stretching speed of 10 mm min^{-1}. Three replicates were conducted for the tensile tests, and the average of the data was reported. The air permeability of cotton fabrics and Ag-Fabric was determined using a fabric permeability tester (YG461E), with circular samples of 10 cm diameter tested under a pressure difference of 100 Pa and a test area of 20 cm^2. The water vapor transmission rate was determined by calculating the evaporative mass loss of the water in the beakers covered with cotton fabric and Ag-fabric, respectively, at a temperature of 37 ℃. The quantitative data with error bars for the air permeability and water vapor transmission rate tests are represented by mean ± standard deviations based on three replicates. For washing test, the samples (3 cm × 3 cm) were placed in a saponification solution (5 g/L soap, 2 g/L sodium carbonate) with a bath ratio of 1:50 and saponified by oscillation at a temperature of 60 °C for 30 min, followed by a washing process in 100 mL saponification solution with stirring using a magnetic stirrer for 30 min. Eight washing cycles were conducted for the samples. The surface wettability was characterized by water contact angle (WCA) using contact angle tester (DSA25, KRUSS). Deionized water of 4 μL was used for each experiment, and the WCA values vesus wetting times were recorded. For each sample, three replicates were conducted and the average of the data was reported.

Antimicrobial property test

The experimental bacteria selected were *Escherichia coli* (*E. coli*), and *Staphylococcus aureus* (*S. aureus*), and these two strains were cultured simultaneously with nutrient broth as the medium. 1 mL of the treated bacterial suspension was pipetted with a pipette gun and added to a sterile Petri dish containing 30 mL of plate-count agar medium. After placing the specimen and the cotton fabric on the agar medium, the sample was incubated at a temperature of 37 °C ± 2 °C for 24 h, ensuring continuous contact between the agar medium and the specimen throughout the incubation period. Finally, the antibacterial activity of the textiles was evaluated by measuring the width of the inhibition zone.

Results and discussion

Functional fabrication and characterization

The easy-to-produce cotton fabric with inherent thermal insulation, wearing comfortability and skin-friendly property was selected as the substrate. PDA-assisted ion deposition technology was harnessed to reduce the silver ion and further deposit AgNPs onto the surface of cotton fibers, forming an human mid-infrared reflective layer; meanwhile, PDA and the localized surface plasmon resonance effect of AgNPs can promote solar energy absorption. Figure 2a

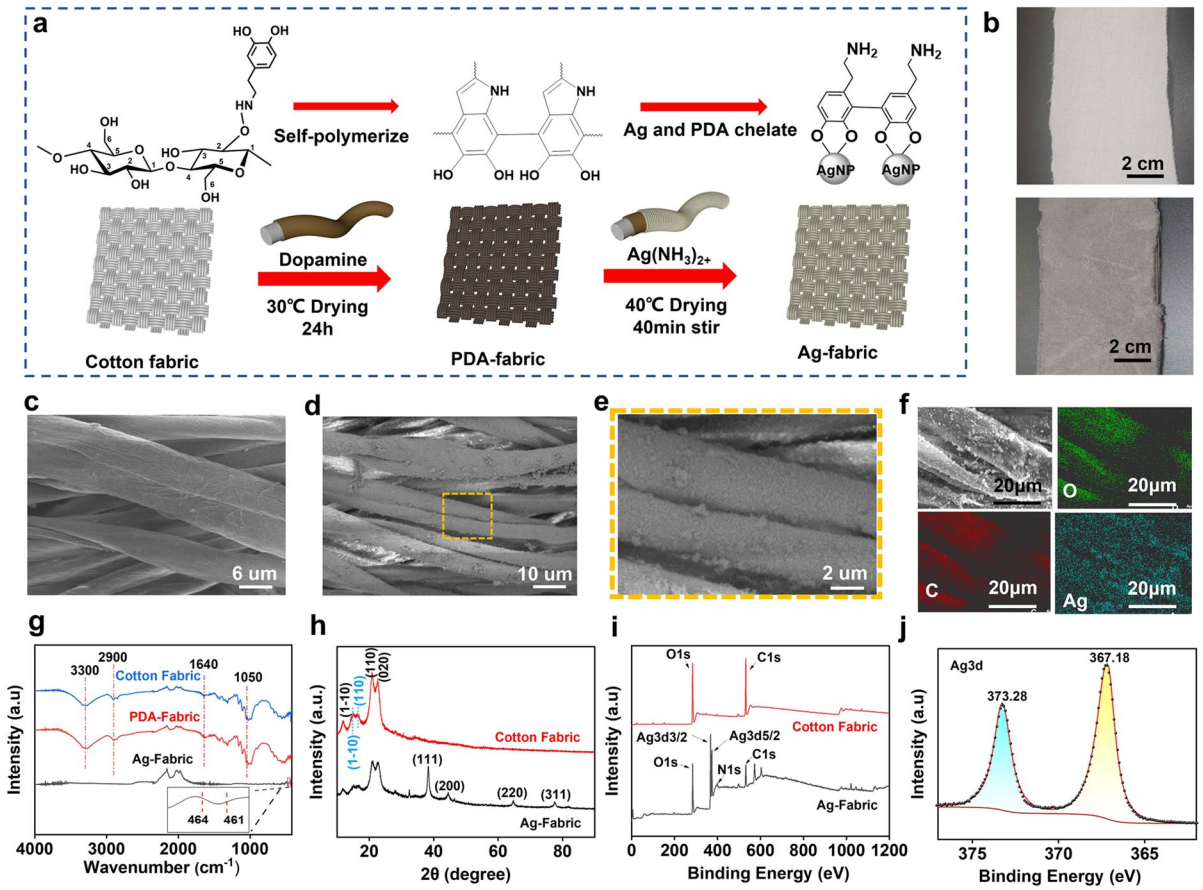

Fig. 2 Fabrication and characterization of the Ag-fabric. **a** Schematic diagram of the Ag-fabric preparation process, along with the reaction mechanism for the PDA polymerization and reduction. **b** Photographs of the unadorned cotton fabric (up) and the Ag-fabric (bottom). (c) SEM images of the PDA-fabric. **d** and **e** SEM images of the Ag-fabric. **f** EDS mapping images of the Ag-fabric. **g** Comparisons of the FTIR spectra among the cotton fabric, PDA-fabric and Ag-fabric. **h** XRD patterns for the cotton fabric and Ag-fabric. The cotton fabric was industrially mercerized during their manufacturing and was further treated with 5 wt% NaOH solution for removing impurities in our pre-treatment process. **i** XPS full spectrum of the cotton fabric and Ag-fabric. **j** High-resolution XPS spectra for Ag 3d

depicts the production process and morphological evolution of the Ag-fabric, which includes the self-polymerization of the DA to form the PDA layer, and the in-situ reduction of AgNPs by PDA-assisted ion deposition on the surface of cotton fibers. Visual inspection of the original cotton textile and modified cotton textile, namely Ag-fabric, is shown in Fig. 2b. The PDA acts as a "bridge" to assist in the deposition of the $AgNP_S$, which automatically aligns with the adhesion mechanism (covalent interaction, hydrogen bonding, ligand interaction) to polymerize into a PDA coating after coming into contact with the cotton surface through Brownian motion in an aerobic, weak alkali environment (Lee et al. 2006; Wang et al. 2020). This PDA coating can be used as a multifunctional secondary reaction platform because the PDA is rich in catechol and amine-reactive groups, which can produce chelation with Ag^+ and significantly promote the adsorption of Ag^+ on cotton fibers (Wu et al. 2023a). Since PDA is mildly reductive, the PDA layer adsorbs the Ag^+ and then reduces to $AgNP_S$ in situ, and these first reduced $AgNP_S$ can be used as a seed layer to promote the formation of subsequent silver coatings (Zeng et al. 2020). Thanks to the chelation and adhesive attraction of the PDA, the silver coating is highly stable in air and water, and durable against water washing, which will be further demonstrated in the following sections. The

unadorned cotton fabric is white and exhibits hierarchical structures ranging from multiple ultrafine and smooth cotton fibers, yarns to weaving construction (Supplementary Fig. S1). Such structures provide the cotton fabric with enough space for the fabrication of micro- and nanoparticles. The self-polymerization of the DA further increases the roughness of the surface of the cotton fibers and provides a desirable platform for the anchoring of the AgNPs (Fig. 2c). To analyze the effect of solution concentration of $AgNO_3$ on the deposition of the AgNPs, different concentrations of $AgNO_3$ solutions of 4, 6, 10, 12, and 16 g/L were prepared. At constant DA solution concentration, the seed layer of AgNPs reduced by PDA remains unchanged, while the amount of the reduced AgNPs increases with the increase of $AgNO_3$ concentration, and the subsequent AgNPs grow and form granular aggregates near the nucleation point. For a relatively low concentration (4 g/L) of $AgNO_3$ solution, most AgNPs are small aggregates with individually dispersed states, and the cotton surface is not entirely covered, leading to a uniformity coating (Supplementary Fig. S2). On the other hand, at the high concentrations (16 g/L) of $AgNO_3$ solution, the $AgNP_S$ grow massively, no longer aggregating along the fiber longitudinal direction but forming larger nanoclusters along the fiber radial direction. This leads to a reduction in uniformity of AgNPs, resulting in an uneven silver coating (Supplementary Fig. S2) (Wei et al. 2022). Finally, the optimized coating with uniform and continuous deposition of AgNPs, as shown in Fig. 2d and e, was achieved by 12 g/L concentrations of $AgNO_3$ solution. Therefore, we chose 12 g/L concentration of $AgNO_3$ solution to prepare the samples hereafter, unless otherwise specified. It is worth noting that the surface pattern of the cotton fabric did not change after modification, and the woven texture still gave a good channel for water vapor permeating. The elemental distribution on the fabric surface was observed by EDS. It can be seen that the distribution of silver elements is as uniform as that of oxygen and carbon elements, indicating that AgNPs are deposited uniformly on the cotton fiber surface (Fig. 2f). Detailed quantitative elemental analyses are shown in Supplementary Fig. S3.

We further studied the bonding mechanism of the silver coatings. The surface chemistry of the cotton fabrics and Ag-fabric were characterized by FT-IR. Since cotton fibers are composed primarily of cellulose, the characteristic peaks of cellulose, such as the –OH stretching vibration at 3300 cm^{-1}, the asymmetric stretching vibration of the $–CH_2$ bond in the cellulose pyran ring appeared at 2900 cm^{-1}, the –OH bending vibration at 1640 cm^{-1} and the C-O stretching vibration at 1050 cm^{-1}, are demonstrated (blue curve in Fig. 2g). The PDA-fabric shows wider absorption peaks, ranging from 3750 to 3000 cm^{-1}, than that of unadorned cotton fabric. The –NH bending vibration absorption peak near 1593 cm^{-1} in the PDA was observed (red curve in Fig. 2g). These results collaboratively indicate that PDA has adhered to the cotton fiber surface. The characteristic peaks of silver (464 cm^{-1} and 461 cm^{-1}) were identified in the black curve of Fig. 2g, demonstrating the successful attachment of AgNPs (Wei et al. 2022). In addition, the significant decrease in the intensity of the peaks for Ag-fabric has been documented, attributed to the extension of AgNPs to the surface of cotton fibers, which attenuates the IR signal (Yue et al. 2019). The crystalline phases of the cotton fabric and Ag-fabric were characterized by XRD. Because cotton fabrics are industrially mercerized during their manufacturing and are further washed with 5 wt% NaOH solution in our pre-treatment process, the cellulose chains are rearranged, changing the crystal form of the cotton from Cellulose Iβ to Cellulose II. It can be seen from Fig. 2h that three diffraction peaks at $2\theta = 12.2°$, 19.9° and 22.1°, correspond to (1–10), (110) and (020) crystal planes of cellulose II, respectively (French 2014). Due to the low concentration of the NaOH solution and the short soaking time (30 min), the crystal form of the cotton is not completely converted into Cellulose II. Therefore, the diffraction peaks corresponding to the (1–10) and (110) crystal planes of cellulose Iβ at 14.6° and 16.6° respectively can still be observed, as indicated by the blue markers in Fig. 2h (Nam et al. 2016). The Ag-fabric shows distinct crystallization peaks at angles of 38.12°, 44.32°, 64.44°, and 77.44°, which corresponds to the (111), (200), (220), and (311) crystal planes of the face-centered cubic crystal structure for the AgNPs, respectively (JCPDS File No. 99-094). Moreover, the Ag-fabric exhibits weakened peaks of cellulose, which can be ascribed to the partial hydrolysis of the cotton fabric caused by the sodium hydroxide solution and the silver-ammonia solution, and the absence of the Ag-O impurity peaks for the Ag-fabric suggests that the reduced AgNPs are in a zero-valent state.

We also used XPS to further confirm the surface chemical composition of the Ag-fabric. Figure 2i compares the XPS spectra of the cotton fabric and Ag-fabric. Several new characteristic peaks appear for the Ag-fabric, indicating the presence of oxygen, nitrogen, silver, and carbon on the surface of Ag-Fabric. The characteristic peak of nitrogen mainly results from the catechol and quinone groups in the PDA polymer, and thus this peak reveals the successful polymerization of PDA in the Ag-fabric. In addition, the Ag 3d XPS spectrum of Ag-fabric deconvolved into two peaks at 367.18 and 373.28 eV for Ag $3d_{5/2}$ and Ag $3d_{3/2}$, respectively, with a distance of about 6.1 eV between the spin energy values, which confirms the presence of silver in the form of Ag (0) (Fig. 2j) (Gu et al. 2020). This result agrees with the data reported for Ag $3d_{5/2}$ and Ag $3d_{3/2}$ in elemental silver, thus confirming the successful reduction of Ag nanoparticles on the surface of cotton fabrics (Xu et al. 2017; Zhu et al. 2018). This conclusion coincides with the results of SEM morphology and XRD spectroscopy.

Radiative heating performance

Passive heating of fabrics, aimed at keeping the human body warm by modulating thermal radiation, is an integral part of personal thermal management. This requires to modify fabrics to be spectrally selective, with typical characteristics such as high absorbance in the solar spectrum (280 ~ 2500 nm) and high reflectivity in the human mid-infrared spectrum (7–14 μm). Polydopamine (PDA) is a mussel-based functional melanin material widely used as a photothermal agent due to its broad light absorption and superior photothermal conversion ability (Chang et al. 2021). In addition, the localized surface plasmon resonance effect allows AgNPs reduced in situ on the surface of cotton fibers to exhibit good spectral absorption in the UV–visible band (Wang et al. 2019a). The combined action of these two materials allows Ag-fabric to effectively absorb solar radiation energy in sunny outdoor environments (Fig. 3a), thus achieving the purpose of keeping warm. Quantitatively, the Ag-fabric shows a high absorptivity of solar power of around 80% corresponding

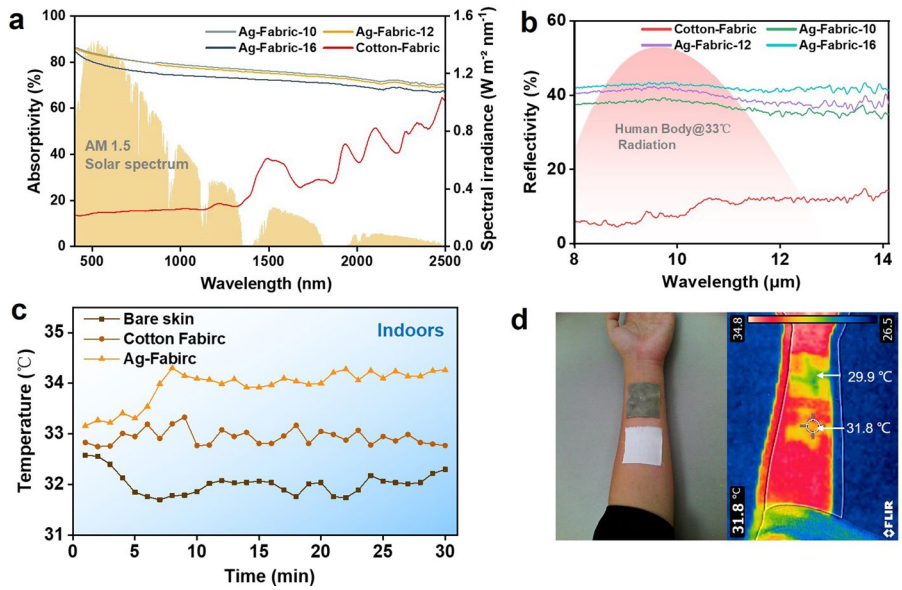

Fig. 3 Radiative heating property characterizations. **a** UV–Vis-NIR absorption spectra of Ag-fabrics and unadorned cotton fabric. The Ag-fabric fabricated under different $AgNO_3$ solution concentrations of $x = 10$, 12 and 16 g/L are denoted by Ag-fabric-x. **b** Mid-infrared reflective spectra of the Ag-fabrics and the unadorned cotton fabric. **c** Temperature evolution of the bare, cotton-fabric-covered and Ag-fabric-12-covered artificial skins in an indoor environment. **d** Infrared and optical images of the Ag-fabric and the cotton fabric. To secure the fabrics onto the arm, we applied adhesive tape at each corner of the fabrics. The uneven color on fabrics may arise from the enhanced thermal conductivity in the taped areas, due to tight contact

to the wavelength range of 400–1350 nm^{-1}, while the absorptivity of the unadorned cotton fabric is pretty low (near zero; the calculation method of the absorptivity is detailed in the Supplementary Note 1). By varying the concentration of $AgNO_3$ solution, the micro-gaps between the AgNPs can be controlled, resulting in different photothermal properties. As shown in Fig. 3a, Ag-Fabric-10, 12, and 16 all exhibit high absorbance in the solar spectrum. However, as the concentration of the silver-ammonia solution increases, the absorption of the solar spectrum decreases instead. This may be attributed to the increased solution concentration, which induces the further growth of AgNPs, forming a dense silver layer. This, in turn, reduces the interconnecting gaps between AgNPs, thereby attenuating the plasmonic near-field coupling effect (Liu et al. 2015; Zhou et al. 2016).

Selective reflection of human radiation is also desirable for heating applications, especially for the indoor environments. According to Planck's law, the human skin, regardless of skin color, can be regarded as a nearly perfect black body that emits electromagnetic radiation in the radiation band with an infrared emissivity of up to 98% (Cai et al. 2018; Hsu et al. 2017; Steketee 1973). Therefore, the wavelength of thermal radiation emitted by the human body is in the mid-infrared band, mainly from 7 to 14 μm, with a peak at 9.5 μm. According to Kirchhoff's law of thermal radiation, the interaction of thermal radiation energy exchange can be expressed by $\varepsilon + T + R = 1$, where ε denotes infrared emissivity, T denotes transmittance, and R denotes reflectivity. Therefore, to achieve the purpose of radiative warming, it is necessary to improve the reflectivity of textiles in the mid-infrared band (Cai et al. 2017). The prepared Ag-fabric shows a broad-spectrum reflectivity up to 40% across the mid-infrared band (Fig. 3b). Moreover, the reflectivity of Ag-fabric to the mid-infrared rises with the increase of AgNPs deposition. This result indicates that the increase of AgNPs has a positive effect on improving the infrared reflectivity of Ag-fabric. By collaboratively considering the comprehensive performance in terms of solar absorption and mid-infrared reflection (Supplementary Fig. S4), we preliminarily chose Ag-Fabric-12 as our ideal sample for subsequent experimental discussion.

To further validate the radiative heating performance of the Ag-fabric, we designed a home-made measurement device for analyzing the skin temperature changes. As shown in Supplementary Fig. S5a, the device consists of thermocouples, an electric heater, and a rubber plate to simulate human skin. At room temperature, the artificial skin was placed on the heater at a constant temperature of 33 °C, and the temperature changes were recorded with thermocouples while covered by the cotton fabric and Ag-fabric, respectively. As shown in Fig. 3c, the temperature of the artificial skin covered by Ag-fabric can reach approximately 34.3 °C, which is higher than that of the skin covered by cotton fabric (average 32.8 °C) and bare skin (average 32.0 °C). The temperature different around 1.5 °C is mainly from the reflection of the radiative heating of human body by the Ag-fabric as illustrated by the model diagram in Supplementary Fig. S5b. We placed both the cotton fabric and the Ag-fabric on the arm and left them for 3 min to ensure the thermal equilibrium with the arm. Then, their surface temperatures were captured using an infrared camera. The infrared images captured by the infrared camera show a temperature difference of outer surfaces between the cotton fabric (31.8 °C) and Ag-fabric (29.9 °C; Fig. 3d), indicating low transmission of human infrared radiation through the Ag-fabric to the surroundings. This suggests the desirable thermal retention performance of the Ag-fabric.

For outdoor environments, converting sunlight into thermal energy can effectively keep thermal comfort of the human body, and is considered an effective energy-saving method. Similar with the indoor measurement device, we designed an outdoor testing device as shown in Fig. 4a, and used an anemometer and a solar power meter to record the environmental factors. The outdoor thermal measurements of Ag-fabric were conducted in April in Wuxi, China, under both sunny and cloudy weather conditions, for up to six hours (Fig. 4b and Supplementary Fig. S5c). On a clear sunny day, the temperature of the artificial skin covered by the Ag-fabric is remarkably higher compared to bare artificial skin and artificial skin covered by the cotton fabric. Throughout the measurement process from 12:00 to 18:00, the artificial skin covered by the Ag-fabric maintained a higher temperature of average 8 °C than that covered by the cotton fabric, under solar irradiance ranging from 800 W m^{-2} to nearly zero, and wind conditions at force levels 1 to 2 (Fig. 4b, c). This temperature enhancement

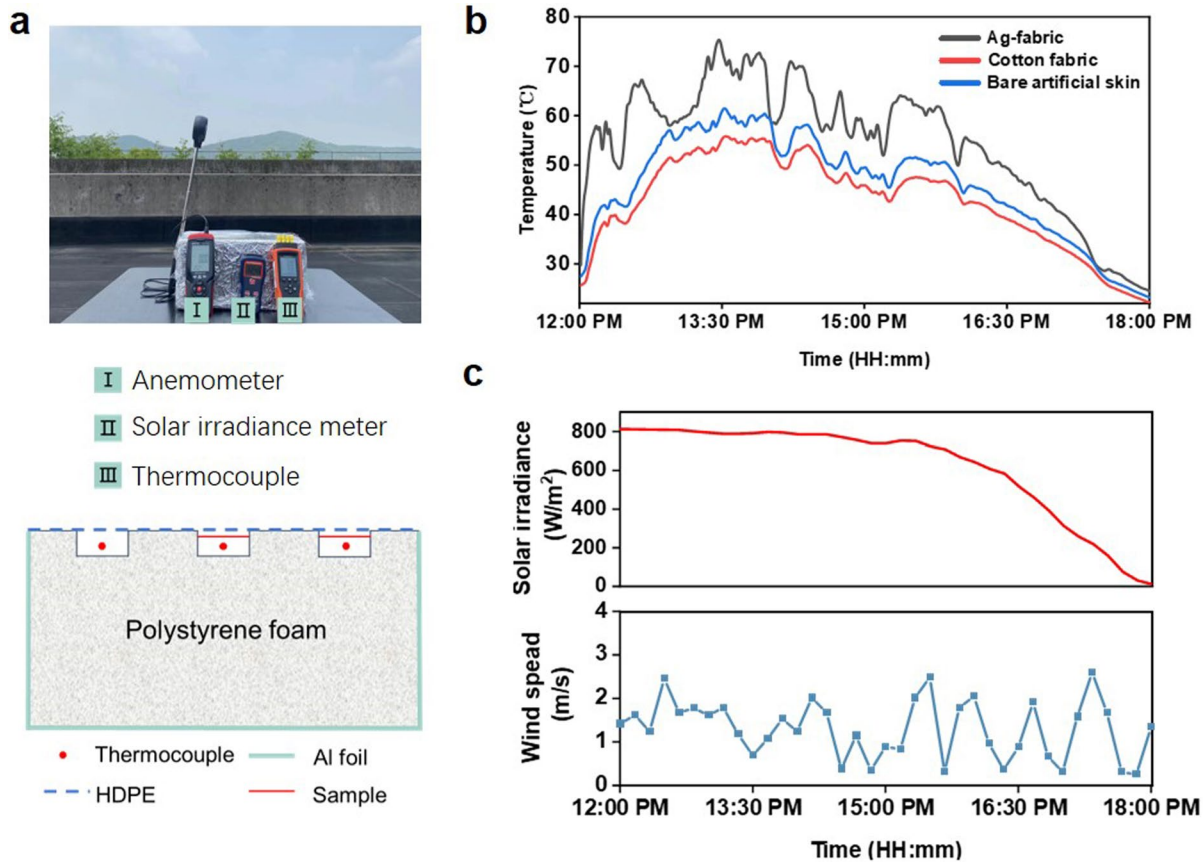

Fig. 4 Outdoor thermal characterization. **a** Setup of the outdoor test device. **b** Real-time temperature profiles of bare, cotton-fabric-covered and Ag-fabric-12-covered artificial skins under direct sunlight on a clear day. **c** Thermal measurement of real-time meteorological parameters

mainly stems from the efficient absorption of sunlight heat by the Ag-fabric. It should be noted that conventional cotton fabrics exhibit relatively high reflectivity (approximately 72%) under direct sunlight (Fig. 4b). In contrast, bare artificial skin with a skin-like color shows relatively low reflectivity and is more efficient at converting light energy into heat energy when exposed to sunlight, resulting in an increase in surface temperature of the bare artificial skin than that covered by cotton fabrics. The temperature difference was reduced on a cloudy day due to the reduced intensity of sunlight affecting the heat absorption of the Ag-fabric, but the Ag-fabrics still showed superior thermal-retention performance than the cotton fabrics. These results demonstrate the great potential of the Ag-fabric for commercial applications in radiative heating wearables.

Electrical heating performance

In complex and cold outdoor environments, achieving human thermal comfort solely through the reflection of body radiation and the light-heat conversion from the sunlight is challenging. Therefore, it is necessary to develop a method that ensures stable heating even in harsh conditions. Electric heating is regarded as a simple and effective method due to its customizability, which shows great potential for applications in providing warmth. The in-situ attachment of AgNPs to the surface of the cotton fabrics endows the Ag-fabric with good electrical conductivity, enabling efficient Joule heating performance (Lee et al. 2020). The electronic resistance of the Ag-fabric decreases with the increase of the $AgNO_3$ solution concentration, as shown in Fig. 5a. However, the electronic resistance

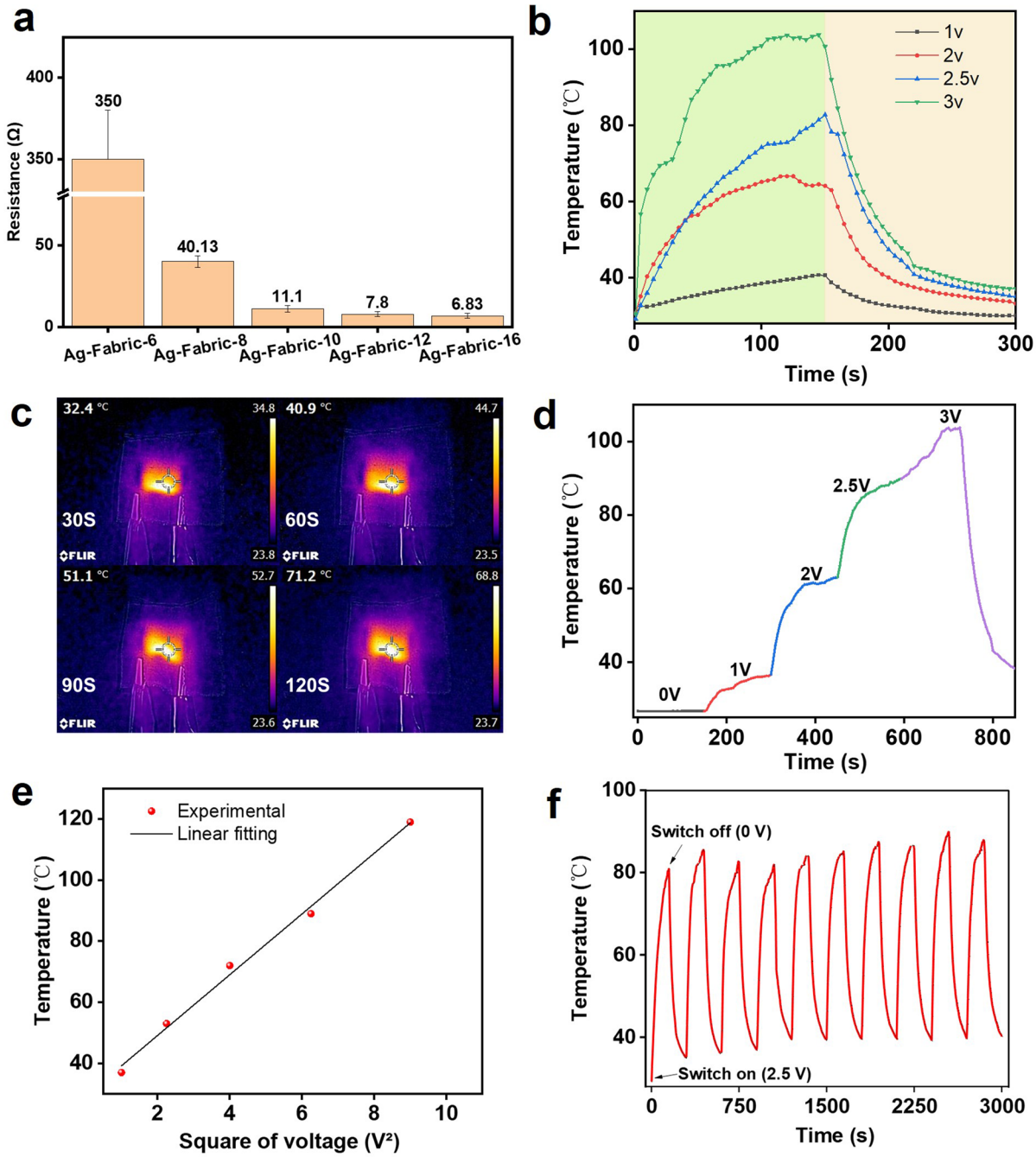

Fig. 5 Electrothermal properties of the Ag-fabric. **a** The electrical resistance of the Ag-fabrics fabricated under different $AgNO_3$ solution concentrations of 6, 10, 12, and 16 g/L. **b** The temperature evolution curves of Ag-fabric-12 under different voltages. **c** Infrared images of the Ag-fabric-12 upon heating at a voltage of 2.5 V for 120 s. **d** Temperature changes of Ag-fabric-12 upon heating under voltages of 0–3 V. **e** Linear relationship between the voltage squared and temperature. **f** The temperature variation of the Ag-fabric-12 during cyclic voltage switching between 0 and 2.5 V

experiences an inflection point in the changes of $AgNO_3$ from 6 to 10 g L^{-1}, beyond which it generally remains stable. To achieve multimodal heating capacity in Ag-fabrics, the Ag-fabric-12 was selected by considering both its radiative heating and electric heating performance collaboratively. It serves as the ideal fabric for achieving optimized thermal-retention performance, and thus is used for further experiments unless specified.

The Ag-fabric exhibits a fast electro-thermal response with the saturation temperature varying from 40 ℃ to over 100 ℃ upon supplied voltages ranging from 1 to 3 V (Fig. 5b). The temperature can reach 40.7 ℃ within 150 s under a supplied voltage of only 1 V. This is safe for human body and efficient for supplying warmth in thermal management wearables. The sequential infrared images of the Ag-fabric surface also demonstrate the temperature changes across the whole fabric (Fig. 5c). Moreover, the saturation temperature of Ag-fabric can be adjusted by changing the supplied voltages (Fig. 5d). The surface saturation temperatures of Ag-fabric reach 40.69 °C, 64.13 °C, 81.4 °C, and 103.72 °C, respectively within 3 min upon applying 1, 2, 2.5, and 3 V voltage, respectively. In addition, the heating saturation temperature shows an approximate linear relationship with the voltage squared (Fig. 5e), which indicates that the resistance remains unchanged during the electric heating process. This provides a convenient way to control the expected temperature by regulating the applied voltages. To examine the heating durability and reliability of the Ag-fabric, we subjected the Ag-fabric to cyclic electrical heating at a maximum voltage of 2.5 V. Figure 5f demonstrates the temperature change curve of the Ag-fabric over 10 cycles in 3000 s. The results show that Ag-Fabric can be heated repeatedly and reaches an approximate saturation temperature at each heating process, indicating the good thermal stability and repeatability of the as-prepared Ag-fabric.

Demonstration of robustness and antibacterial property.

As a wearable textile, the breathability, mechanical strength, washability, and durability of the Ag-fabric are necessary for practical applications. The water vapor transmission rate testing reveals the excellent breathability of Ag-fabric, which is comparable to that of original cotton fabric (Fig. 6a). This is because the in-situ polymerization of AgNPs on cotton fabrics does not mask the interlocking texture of the woven fabrics. The air permeability of the Ag-fabric is slightly lower than that of the cotton fabric as the AgNPs adhesion slightly shortens the gap between the fibers; whereas, the Ag-fabric still maintains good air permeability over 160 mm/s (Fig. 6b). The breaking strength (17.95 MPa) and breaking elongation (12.68%) of the Ag-fabric are comparable to that of the cotton fabric and even slightly higher than that of original cotton fabric due to the adhesion of AgNPs (Fig. 6c). This mechanical strength can fulfill the daily application. Figure 6d compares the water contact angles on the surface of the cotton fabric and Ag-fabric, indicating the hydrophobicity of the Ag-fabric. Notably, the different liquid droplets, such as tea, milk, coffee, juice, and soda, remain nearly spherical on the fabric surface rather than being absorbed (Supplementary Fig. S6a, b), demonstrating the good self-cleaning property of the Ag-fabric. Moreover, the Ag-fabric show robust performance against cyclic washing and wearing. As shown in Fig. 6e and f, the solar absorptivity, infrared reflectivity, and electrical conductivity of the Ag-fabric show less change compared with the original samples after several washing cycles. In addition, good abrasion resistance of the Ag-fabric is confirmed by the wearing tests (Fig. 6f). The SEM images of the fiber surfaces for washed, twisted and rubbed Ag-fabric in the Supplementary Fig. S7 further demonstrate the excellent durability of the Ag-fabric. This is mainly ascribed to the interfacial layer PDA, whose superb interfacial adhesion allows the metal nanoparticles to bind tightly to the cotton fibers, thus ensuring long-term mechanical properties and durability.

Moreover, it is inevitably for humans to be exposed to humid environments, making it easy for bacteria to grow and thus jeopardizing human health. Therefore, we chose *E. coli* and *S. aureus* as the representative strains to investigate the antimicrobial performance of Ag-fabric and cotton-fabric and evaluated the antibacterial effect of the fabrics in terms of the size of the radius of the inhibition circle. As shown in Fig. 6g, no inhibitory circle appeared around cotton-fabric on the medium of *E. coli* and *S. aureus*, indicating that the cotton-fabric had no inhibitory activity. On the contrary, 14 mm and 15 mm inhibition circles appears around Ag-fabric, respectively, which reveals the excellent antibacterial performance of Ag-fabric. This is

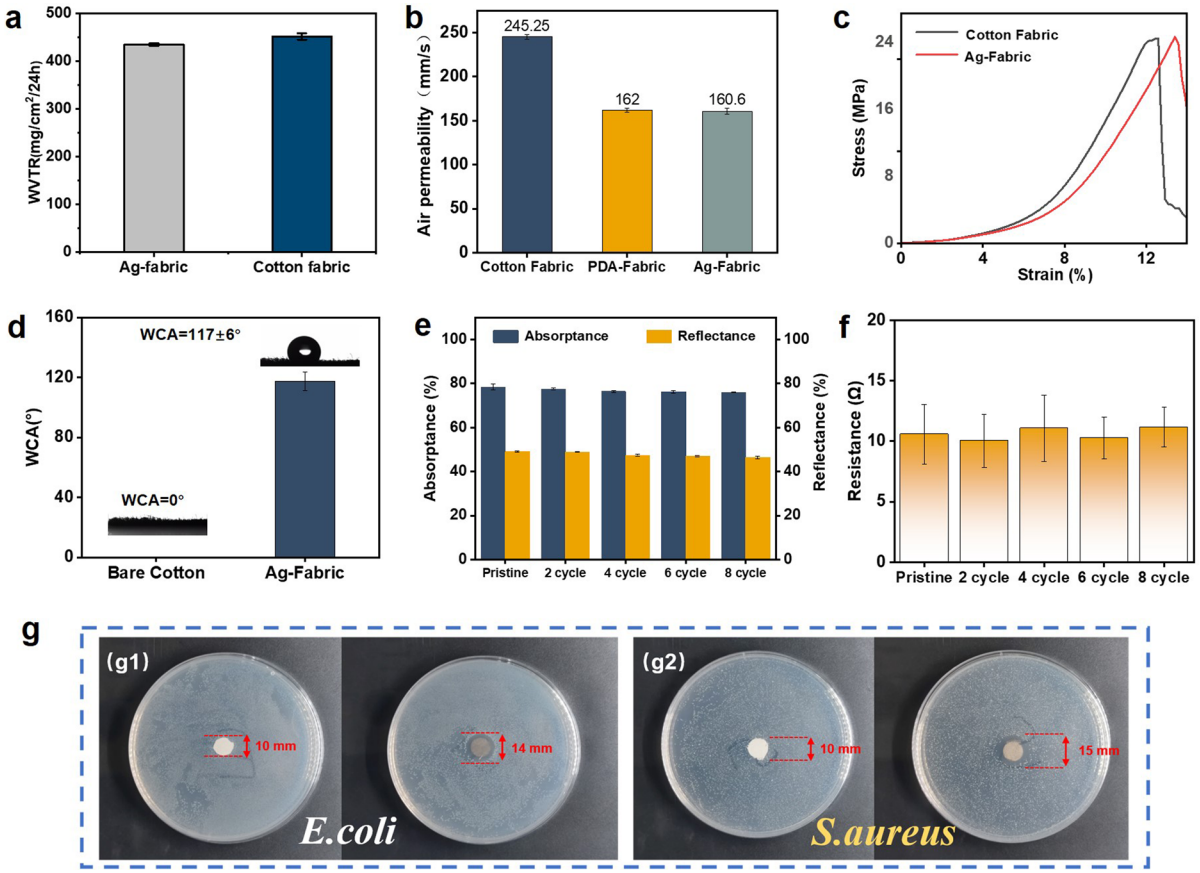

Fig. 6 The breathability, durability and antibacterial property of the Ag-fabric. **a** Comparisons of the water vapor transmission rate (WVTR) of the cotton fabric and Ag-fabric. **b** Comparisons of the air permeability of the cotton fabric and Ag-fabric. **c** Tensile properties of the cotton fabric and Ag-fabric. **d** Contact angle test for the Ag-fabric and cotton fabric. **e** The washing durability of the Ag-fabric characterized by the absorption in the solar spectrum and reflection in the mid-infrared over 8 washing cycles. **f** The abrasion resistance of the Ag-fabric evaluated by the changes in the electrical resistance of the Ag-fabric over cyclic wearing tests. **g** Comparison of the antibacterial properties of the Ag-fabric (right) and cotton fabric (left)

attributed to the silver ions released by AgNPs on the surface of cotton fibers. These ions can damage cellular DNA molecules and certain proteases, leading to cross-linking of DNA molecules or catalyzing the formation of free radicals. As a result, viral proteins denature, and electron donors on DNA molecules are inhibited, resulting in DNA strand breakage and cell death (Sotiriou and Pratsinis 2010; Vigneswari et al. 2021; Xie et al. 2019). As Ag-Fabric possesses excellent antibacterial properties, it avoids degradation and damage of Ag-fabric caused by bacteria. This not only preserves human health but also extends lifespan of the fabric.

Conclusions

We have demonstrated multimodal heating Ag-fabrics with robust durability, excellent comfort, and antibacterial property by tightly integrating AgNPs with cotton fibers through a PDA-assisted ion deposition technique. The chelation and adhesive effects of the PDA ensure the high robustness and durability of the silver coating, even when subjected to cyclic washing, twisting, and rubbing. The as-prepared Ag-fabric can achieve a temperature of almost 2 ℃ higher than unadorned cotton fabrics in an indoor environment, and can achieve an increase of average 8 ℃ for artificial skin covered by the Ag-fabric, compared with that

covered by unadorned cotton fabrics under sunlight. In addition, the textile shows significant Joule heating capacity, antibacterial properties, and self-cleaning property, while maintaining good breathability, water vapor permeability and mechanical strength. It is believed that our study can not only promote the practical applications of cotton fabrics for the new generation of thermal insulation clothing, but also provide new insights into processing natural materials through facile and convenient method for multifunctional thermal management wearables.

Acknowledgments The authors gratefully thank the financial support from the National Natural Science Foundation of China (Grant Numbers 12272149 and 11802104), the China Postdoctoral Science Foundation (Grant Number 2023M741400), and the National Key Research and Development Program (Grant Number 2017YFB0309200). We thank Dr. Kunkun Zhu (Wuhan Textile University) for his helpful discussion on the chemical structure of cellulose. We also appreciate Prof. Alfred French and the anonymous reviewers for their valuable comments and suggestions on our manuscript.

Author contributions B. Li, F. Sun and X. Su contributed to the study conception and design. Material preparation, experimental investigation and analysis were performed by B. Li, S. Ao, H. Song and C. Liu. The first draft of the manuscript was written by B. Li and all authors commented on previous versions of the manuscript. All authors read and approved the final manuscript.

Funding This work was supported by the National Natural Science Foundation of China (Grant Numbers 12272149 and 11802104), the China Postdoctoral Science Foundation (Grant Number 2023M741400), and the National Key Research and Development Program (Grant Number 2017YFB0309200). X. Su has received research support from Shenzhen Purcotton Technology Co., Ltd (China).

Data availability No datasets were generated or analysed during the current study.

Declarations

Competing interests The authors declare no competing interests.

Consent for publication All authors agree to this publication.

References

Alves O, Monteiro E, Brito P, Romano P (2016) Measurement and classification of energy efficiency in HVAC systems. Energy Build 130:408–419. https://doi.org/10.1016/j.enbuild.2016.08.070

Axelrod YK, Diringer MN (2006) Temperature management in acute neurologic disorders. Crit Care Clin 22(4):767–. https://doi.org/10.1016/j.ccc.2006.06.001

Cai L, Song AY, Wu P, Hsu PC, Peng Y, Chen J, Liu C, Catrysse PB, Liu Y, Yang A, Zhou C, Zhou C, Fan S, Cui Y (2017) Warming up human body by nanoporous metallized polyethylene textile. Nat Commun 8(1):496. https://doi.org/10.1038/s41467-017-00614-4

Cai L, Song AY, Li W, Hsu PC, Lin D, Catrysse PB, Liu Y, Peng Y, Chen J, Wang H, Xu J, Yang A, Fan S, Cui Y (2018) Spectrally selective nanocomposite textile for outdoor personal cooling. Adv Mater 30(35):e1802152. https://doi.org/10.1002/adma.201802152

Chang Q, Guo ZY, Shen ZH, Li N, Xue CR, Zhang HN, Hao CH, Yang JL, Hu SL (2021) Interaction promotes the formation and photothermal conversion of carbon dots/polydopamine composite for solar-driven water evaporation. Adv Mater Interfaces 8(12):7. https://doi.org/10.1002/admi.202100332

Fang DD (2018) General description of cotton. In: Fang DD (ed) Cotton fiber: physics, chemistry and biology. Springer, Cham, pp 1–11

French AD (2014) Idealized powder diffraction patterns for cellulose polymorphs. Cellulose 21(2):885–896. https://doi.org/10.1007/s10570-013-0030-4

Gao G, Shi J-W, Fan Z, Gao C, Niu C (2017) MnM_2O_4 microspheres (M = Co, Cu, Ni) for selective catalytic reduction of no with NH_3: comparative study on catalytic activity and reaction mechanism via in-situ diffuse reflectance infrared Fourier transform spectroscopy. Chem Eng J 325:91–100. https://doi.org/10.1016/j.cej.2017.05.059

Gong S, Sheng XX, Li XL, Sheng MJ, Wu H, Lu X, Qu JP (2022) A multifunctional flexible composite film with excellent multi-source driven thermal management, electromagnetic interference shielding, and fire safety performance, inspired by a brick-mortar sandwich structure. Adv Funct Mater 32(26):12. https://doi.org/10.1002/adfm.202200570

Gu B, Huang XY, Qiu FX, Yang DY, Zhang T (2020) Laminated cellulose hybrid membranes with triple thermal insulation functions for personal thermal management application. ACS Sustain Chem Eng 8(42):15936–15945. https://doi.org/10.1021/acssuschemeng.0c05465

Hong S, Gu Y, Seo JK, Wang J, Liu P, Meng YS, Xu S, Chen RK (2019) Wearable thermoelectrics for personalized thermoregulation. Sci Adv 5(5):11. https://doi.org/10.1126/sciadv.aaw0536

Hsu PC, Liu XG, Liu C, Xie X, Lee HR, Welch AJ, Zhao T, Cui Y (2015) Personal thermal management by metallic nanowire-coated textile. Nano Lett 15(1):365–371. https://doi.org/10.1021/nl5036572

Hsu PC, Liu C, Song AY, Zhang Z, Peng YC, Xie J, Liu K, Wu CL, Catrysse PB, Cai LL, Zhai S, Majumdar A, Fan SH, Cui Y (2017) A dual-mode textile for human body radiative heating and cooling. Sci Adv 3(11):8. https://doi.org/10.1126/sciadv.1700895

Karim N, Afroj S, Lloyd K, Oaten LC, Andreeva DV, Carr C, Farmery AD, Kim ID, Novoselov KS (2020) Sustainable personal protective clothing for healthcare applications: a review. ACS Nano 14(10):12313–12340. https://doi.org/10.1021/acsnano.0c05537

Khan BA, Chevali VS, Na HN, Zhu J, Warner P, Wang H (2016) Processing and properties of antibacterial silver nanoparticle-loaded hemp hurd/poly(lactic acid) biocomposites. Compos Pt B Eng 100:10–18. https://doi.org/10.1016/j.compositesb.2016.06.022

Lan CT, Xu F, Pan CX, Guo ZH, Pu X (2023) Mxene based janus fabrics with radiative heating towards efficient personal thermal management. Chem Eng J 472:7. https://doi.org/10.1016/j.cej.2023.144662

Lee H, Scherer NF, Messersmith PB (2006) Single-molecule mechanics of mussel adhesion. Proc Natl Acad Sci USA 103(35):12999–13003. https://doi.org/10.1073/pnas.0605552103

Lee J, Llerena Zambrano B, Woo J, Yoon K, Lee T (2020) Recent advances in 1d stretchable electrodes and devices for textile and wearable electronics: materials, fabrications, and applications. Adv Mater 32(5):e1902532. https://doi.org/10.1002/adma.201902532

Li JL, Cai JY, Yu JY, Li ZL, Ding B (2023) The rising of fiber constructed piezo/triboelectric nanogenerators: from material selections, fabrication techniques to emerging applications. Adv Funct Mater 33(44):31. https://doi.org/10.1002/adfm.202303249

Liu ZQ, Liu XS, Huang S, Pan PP, Chen J, Liu GQ, Gu G (2015) Automatically acquired broadband plasmonic-metamaterial black absorber during the metallic film-formation. ACS Appl Mater Interfaces 7(8):4962–4968. https://doi.org/10.1021/acsami.5b00056

Nam S, French AD, Condon BD, Concha M (2016) Segal crystallinity index revisited by the simulation of X-ray diffraction patterns of cotton cellulose Iβ and cellulose II. Carbohydr Polym 135:1–9. https://doi.org/10.1016/j.carbpol.2015.08.035

Peng YC, Cui Y (2020) Advanced textiles for personal thermal management and energy. Joule 4(4):724–742. https://doi.org/10.1016/j.joule.2020.02.011

Sotiriou GA, Pratsinis SE (2010) Antibacterial activity of nanosilver ions and particles. Environ Sci Technol 44(14):5649–5654. https://doi.org/10.1021/es101072s

Steketee J (1973) Spectral emissivity of skin and pericardium. Phys Med Biol 18(5):686–694. https://doi.org/10.1088/0031-9155/18/5/307

Tang LT, Lyu B, Gao DG, Jia ZT, Fu YT, Ma JZ (2023) A Janus textile with tunable heating modes toward precise personal thermal management in cold conditions. Small. https://doi.org/10.1002/smll.202308194

Tian TH, Wei XDA, Elhassan A, Yu JY, Li ZL, Ding B (2021) Highly flexible, efficient, and wearable infrared radiation heating carbon fabric. Chem Eng J 417:7. https://doi.org/10.1016/j.cej.2020.128114

Vigneswari S, Amelia TSM, Hazwan MH, Mouriya GK, Bhubalan K, Amirul AA, Ramakrishna S (2021) Transformation of biowaste for medical applications: incorporation of biologically derived silver nanoparticles as antimicrobial coating. Antibiotics-Basel 10(3):22. https://doi.org/10.3390/antibiotics10030229

Wang LL, Zhu GH, Wang M, Yu W, Zeng J, Yu XX, Xie HQ, Li Q (2019a) Dual plasmonic Au/TiN nanofluids for efficient solar photothermal conversion. Sol Energy 184:240–248. https://doi.org/10.1016/j.solener.2019.04.013

Wang X, Liu QC, Wu SY, Xu BX, Xu HX (2019b) Multilayer polypyrrole nanosheets with self-organized surface structures for flexible and efficient solar-thermal energy conversion. Adv Mater 31(19):9. https://doi.org/10.1002/adma.201807716

Wang Z, Zou Y, Li YW, Cheng YY (2020) Metal-containing polydopamine nanomaterials: catalysis, energy, and theranostics. Small 16(18):21. https://doi.org/10.1002/smll.201907042

Wang YT, Peng HK, Li TT, Shiu BC, Ren HT, Zhang XF, Lou CW, Lin JH (2021) Mxene-coated conductive composite film with ultrathin, flexible, self-cleaning for high-performance electromagnetic interference shielding. Chem Eng J 412:13. https://doi.org/10.1016/j.cej.2021.128681

Wang J, Ma XY, Zhou JL, Du FL, Teng C (2022) Bioinspired, high-strength, and flexible mxene/aramid fiber for electromagnetic interference shielding papers with joule heating performance. ACS Nano 16(4):6700–6711. https://doi.org/10.1021/acsnano.2c01323

Wei WT, Zhang PF, Cao F, Liu JH, Qian K, Pan DK, Yao YT, Li WB (2022) Ultrathin flexible electrospun eva nanofiber composite with electrothermally-driven shape memory effect for electromagnetic interference shielding. Chem Eng J 446:11. https://doi.org/10.1016/j.cej.2022.137135

Wu JJ, Wang MX, Dong L, Zhang Y, Shi J, Ohyama M, Kohsaka Y, Zhu CH, Morikawa H (2023a) Highly integrated, breathable, metalized phase change fibrous membranes based on hierarchical coaxial fiber structure for multimodal personal thermal management. Chem Eng J 465:11. https://doi.org/10.1016/j.cej.2023.142835

Wu M, Shao Z, Zhao N, Zhang R, Yuan G, Tian L, Zhang Z, Gao W, Bai H (2023b) Biomimetic, knittable aerogel fiber for thermal insulation textile. Science (New York, NY) 382(6677):1379–1383. https://doi.org/10.1126/science.adj8013

Xie YJ, Yue LN, Zheng YD, Zhao L, Liang CY, He W, Liu ZW, Sun Y, Yang YY (2019) The antibacterial stability of poly(dopamine) in-situ reduction and chelation nano-ag based on bacterial cellulose network template. Appl Surf Sci 491:383–394. https://doi.org/10.1016/j.apsusc.2019.06.096

Xu JW, Xu N, Zhou T, Xiao X, Gao B, Fu JJ, Zhang TC (2017) Polydopamine coatings embedded with silver nanoparticles on nanostructured titania for long-lasting antibacterial effect. Surf Coat Technol 320:608–613. https://doi.org/10.1016/j.surfcoat.2016.10.065

Yang CQ, Zhou WL, Lickfield GC, Parachura K (2003) Cellulase treatment of durable press finished cotton fabric: effects on fabric strength, abrasion resistance, and handle. Text Res J 73(12):1057–1062. https://doi.org/10.1177/004051750307301205

Yang P, He JJ, Ju YS, Zhang QY, Wu YP, Xia ZC, Chen L, Tang SC (2023) Dual-mode integrated janus films with highly efficient enhanced infrared radiative cooling and solar heating for year-round thermal management. Adv Sci 10(7):10. https://doi.org/10.1002/advs.202206176

Yue X, Zhang T, Yang D, Qiu F, Li Z, Wei G, Qiao Y (2019) Ag nanoparticles coated cellulose membrane with high infrared reflection, breathability and antibacterial property for human thermal insulation. J Colloid Interface Sci 535:363–370. https://doi.org/10.1016/j.jcis.2018.10.009

Yue XJ, He MY, Zhang T, Yang DY, Qu FX (2020) Laminated fibrous membrane inspired by polar bear pelt for outdoor personal radiation management. ACS Appl Mater Interfaces 12(10):12285–12293. https://doi.org/10.1021/acsami.9b20865

Zeng ZH, Jiang FZ, Yue Y, Han DX, Lin LC, Zhao SY, Zhao YB, Pan ZY, Li CJ, Nystrom G, Wang J (2020) Flexible and ultrathin waterproof cellular membranes based on high-conjunction metal-wrapped polymer nanofibers for electromagnetic interference shielding. Adv Mater 32(19):7. https://doi.org/10.1002/adma.201908496

Zhao DL, Lu X, Fan TZ, Wu YS, Lou L, Wang QW, Fan JT, Yang RG (2018) Personal thermal management using portable thermoelectrics for potential building energy saving. Appl Energy 218:282–291. https://doi.org/10.1016/j.apenergy.2018.02.158

Zhou L, Tan YL, Ji DX, Zhu B, Zhang P, Xu J, Gan QQ, Yu ZF, Zhu J (2016) Self-assembly of highly efficient, broadband plasmonic absorbers for solar steam generation. Sci Adv 2(4):8. https://doi.org/10.1126/sciadv.1501227

Zhu YL, Chi Y, Liang SE, Luo X, Chen KP, Tian CR, Wang JH, Zhang L (2018) Novel metal coated nanoencapsulated phase change materials with high thermal conductivity for thermal energy storage. Sol Energy Mater Sol Cells 176:212–221. https://doi.org/10.1016/j.solmat.2017.12.006